www.nature.com/aps

Acta Pharmacologica Sinica

ARTICLE

Activation of SIRT1 ameliorates LPS-induced lung injury in mice via decreasing endothelial tight junction permeability

Cuiping Fu[1], Shengyu Hao[1], Xiaobo Xu[1], Jian Zhou[1], Zilong Liu[1], Huan Lu[1], Limin Wang[2], Weizhong Jin[2] and Shanqun Li[1]

The integrity of the endothelial barrier is a determinant of the prognosis of lipopolysaccharide (LPS)-induced acute lung injury (ALI). In this study, we investigated whether and how Sirtuin 1 (SIRT1) maintained the vascular integrity during ALI. An experimental model of ALI was established in mice through intratracheal administration of LPS (10 mg/kg). LPS stimulation significantly increased the pulmonary permeability and decreased the expression of SIRT1 and tight junction proteins (TJs), including occludin, claudin-5, tight junction protein 1 and tight junction protein 2. Morphological studies showed that LPS induced obvious lung injury with inflammatory cell infiltration in the interstitial and alveolar space, hemorrhage, edema, and the thickened alveolar wall compared to the control mice. Intratracheal administration of the selective SIRT1 activator SRT1720 (6.25 mg/kg) significantly attenuated LPS-induced lung injury, lung hyper-permeability and increased TJs expression, whereas intratracheal administration of the selective SIRT1 inhibitor EX527 (6.25 mg/kg) aggravated LPS-induced ALI. Similar protective effects of SIRT1 on pulmonary cellular permeability were observed in primary human pulmonary microvascular endothelial cells treated with LPS (2 mg/mL) in vitro. We further demonstrated that the RhoA/ROCK signaling pathway was activated in SIRT1 regulation of tight junction permeability. The RhoA/ROCK inhibitor Y-27632 (10 μM) increased the expression of TJs and reversed LPS- or EX527-induced hyper-permeability. In conclusion, SIRT1 ameliorates LPS-induced lung injury via decreasing endothelial tight junction permeability, possibly via RhoA/ROCK signaling pathway. This finding may contribute to the development of new therapeutic approaches for lung injury.

Keywords: lung injury; LPS; SIRT1 protein; RhoA/ROCK; capillary endothelial permeability; tight junction proteins; SRT1720; EX527; Y-27632; human pulmonary microvascular endothelial cells

Acta Pharmacologica Sinica (2019) 40:630–641; https://doi.org/10.1038/s41401-018-0045-3

INTRODUCTION

Acute lung injury (ALI) is a critical illness characterized by acute respiratory distress, hypoxemia, and non-cardiogenic pulmonary edema. Lipopolysaccharide (LPS), the major constituent of the outer membrane of Gram-negative bacteria, is a well-known inducer of lung injury and has been used to model ALI [1–3]. LPS is also commonly used to stimulate lung injury in mice and induces inflammation in various cell types [4]. Despite advances in the airway management and protective ventilation strategies, the mortality rate among ALI patients remains high (~40%) because the mechanisms underlying ALI pathogenesis remain unclear [5].

Inflammation is a key factor of ALI; however, studies demonstrated that anti-inflammation in the lung could not reverse ALI completely. Increased lung vascular permeability is another key feature of ALI in septic patients, which typically develops in concert, leading to progressive deterioration of lung function [6]. The pathophysiology of lung injury is still considered more of an inflammation response after several decades of research. Extensive efforts and numerous studies in this field have proved fruitful in revealing important mechanisms that are involved in the development of this devastating disease, yet a complete understanding of the entire pathological process is lacking. The discovery of specific molecular participation in permeability barrier damage has caused attention. Endothelial dysfunction and pulmonary microvascular hyper-permeability to fluids and proteins are the hallmarks of ALI [7]. Thus, stable pulmonary permeability has been developed as a potential therapeutic strategy of ALI. The integrity of the endothelial cell monolayer directly determines lung vascular permeability given that the endothelial barrier between the vessel lumen and underlying alveoli mediates the transmigration of blood cells and macromolecules and maintains lung fluid homeostasis [8]. However, the mechanism of lung hyper-permeability during ALI is not completely clear to date.

Underlying mechanisms of hyper-permeability in ALI remain elusive. Pulmonary permeability is decided by intercellular junctions, including gap junctions, adhering junctions, and tight junctions. These junctions perform numerous roles, including regulating cellular permeability in ALI [9]. As one of the important components of the special structure of the capillary-alveolar barrier, tight junctions are essential for maintaining a stable pulmonary microenvironment [10]. Occludin, claudins, tight junction protein 1 (ZO-1), and tight junction protein 2 (ZO-2) are key members of tight junction proteins (TJs). Occludin is a primary

[1]Department of Pulmonary Medicine, Clinical Center for Sleep Breathing and Snoring, Zhongshan Hospital of Fudan University, Shanghai 200032, China and [2]Department of Pulmonary Medicine, Hangzhou First People's Hospital, Nanjing Medical University, Hangzhou 310006, China
Correspondence: Shanqun Li (lsq18616880856@163.com) or Weizhong Jin (wzkingfdu@163.com)
These authors contributed equally: Cuiping Fu, Shengyu Hao

Received: 25 November 2017 Accepted: 12 May 2018
Published online: 18 July 2018

transmembrane protein consisting of four transmembrane domains, two extracellular loops and three cytoplasmic domains. The unique charged structures of the extracellular loops may enable cells to attach to each other [11]. ZO-1 interacts directly with transmembrane factors, including claudins, occludin, and unctional adhesion molecule-A, and ZO-1 organizes and regulates the structure of tight junctions [12]. To develop effective therapeutic strategies, we further explored the molecular mechanisms underlying pathogenic conditions related to microvascular hyper-permeability.

Proteases, reactive oxygen species, and matrix metalloproteinases released during inflammatory responses increase lung permeability [13–15]. However, no specific molecule could be effectively translated to clinical application. Sirtuin 1 (SIRT1), a nicotinamide adenine dinucleotide-dependent class III histone deacetylase, is a mammalian Sir2 homologue in the yeast *Saccharomyces cerevisiae*. SIRT1 is involved in a number of pathophysiological processes, including anti-inflammation [16, 17], DNA damage repair, apoptosis inhibition, oxidative stress resistance, and cell lifespan extension [18]. According to recent studies, several drugs protected lung injury through activating SIRT1 [19, 20]. Knockdown of SIRT1 leads to increased inflammatory cytokine release, whereas SIRT1 activation inhibits the production of these cytokines [21]. On the other hand, studies demonstrated that resveratrol alleviated pulmonary edema through activation of SIRT1 [22]. Increased expression of endogenous SIRT1 might play a neuroprotective role against brain vascular hyper-permeability after subarachnoid hemorrhage [23]. This finding suggests that SIRT1 could be a potential target for the regulation of ALI and indicates the role of SIRT1 in vascular permeability. In this study, the effects and potential mechanisms of SIRT1 on micro-vascular hyper-permeability induced by LPS challenge were investigated in vivo and in vitro to better understand the pathogenesis of sepsis-induced ALI and to explore better potential therapeutic options for ALI.

MATERIALS AND METHODS

Animals and experiment group

Balb/c mice (Lingchang Biotech Corporation, Shanghai, China) used in this study were at 8–12 weeks of age and were age- and sex-matched with controls in the experiment. Experimental protocols were approved by the Animal Care Committee of Fudan University. Mice were randomly assigned to six groups: control group, EX527 group, SRT1720 group, LPS group, LPS plus EX527 group, and LPS plus SRT1720 group. The general procedure modeling LPS-induced lung injury has been described in a previous study from our lab [24]. Briefly, mice were anesthetized and placed in a supine position head up on a tilted board. Lipopolysaccharide from *Escherichia coli* O55:B5 (Sigma, USA) was dissolved in 0.9% saline and orally instilled to the trachea at a dosage of 10 mg/kg with a 22-gauge feeding needle (Terumo, Tokyo, Japan). Then, mice were placed in a vertical position and rotated for 30 s to distribute the LPS evenly within the lungs. Mice in control group received the same volume of 0.9% saline and manipulations. For EX527/SRT1720 intratracheal treatment, the same protocol as LPS instillation as described above was adopted. Mice were injected intratracheally with EX527/SRT1720 at the indicated doses alone or accompanied with LPS as previously described [25]. For SIRT1 inhibition, 6.25 mg/kg of EX527 (Selleck, Houston, USA) was used and administered intratracheally given that this schedule was demonstrated to inhibit SIRT1 in the lung. For SIRT1 activation, 6.25 mg/kg of SRT1720 (Selleck, Houston, USA) was used and administered intratracheally as previously described. All mice were euthanized at 12 h after drugs or saline administration.

Evans blue dye extravasation assay

Lung capillary leakage in mice was assessed by Evans blue dye extravasation using a technique modified from a previously published technique [26]. Briefly, Evans blue (Sigma, Samoa, USA) dye (30 mg/kg) was injected via the internal jugular vein into mice 3 h before euthanasia. A heparinized syringe was administered to mice, and then mice were sacrificed. Blood was drawn from the cardiac apex using an injector. Blood was centrifuged at 4500 rpm, and plasma was retained for Evans blue detection measured at 620 nm by a microplate reader. The right ventricle was perfused with phosphate-buffered saline (PBS) to remove intravascular dye from the lungs. The entire lung was removed and placed in formamide (Sigma–Aldrich, USA, formamide is a type of solvent that extracts Evans blue from lung), and blood was eliminated during this process. Evans blue was extracted by the addition of 4 mL of formamide followed by incubation for 72 h in a tube at 60 °C. After centrifugation at $5000 \times g$ for 30 min, the absorption of Evans blue in lung supernatants was measured at 620 nm and corrected for the presence of hemepigments as follows: A620 (corrected) = A620 − (1.426 × A740 + 0.030) [26]. The Evans blue index was calculated as the ratio of the amount of dye in the lungs to the plasma dye concentration.

Bronchoalveolar lavage fluid

Bronchoalveolar lavage fluid (BALF) was harvested from both the right and left lungs [27]. The supernatant was harvested after centrifugation at $12{,}000 \times g$ for 30 min for further analysis, and total protein concentration in the supernatant was measured using the BCA test kit (Beyotime, Shanghai, China).

Lung wet-to-dry weight ratio

The lung wet-to-dry weight ratio was used as an index of pulmonary edema formation that served as a gauge for measuring lung injury and pulmonary permeability. Lung tissues were weighed immediately after removal (wet weight) and then placed into a 60 °C oven for 48 h. The dried lung portion was reweighed (dry weight). The ratio of the lung weight before and after drying was calculated.

Lung histopathologic examination

For histopathological analysis, lung tissues were fixed with 10 % formalin and embedded in paraffin, and 5-μm sections were stained with hematoxylin and eosin (H&E). The total surface of the slides was scored by two blinded pathologists with expertise in lung pathology. The degree of microscopic injury was evaluated on the basis of the following variables: edema of alveolar and interstitial, inflammatory infiltration, and hemorrhage (Table 1). A total of three slides from each lung sample was randomly screened, and the mean was obtained as the representative value of the sample [28].

Cell culture, treatment, and transfection

Primary human pulmonary microvascular endothelial cells (HPMECs) were obtained from ScienCell Research Laboratories and were maintained in ScienCell Endothelial Cell Medium with 5% fetal bovine serum in a humidified incubator at 37 °C with 5%

Table 1. Criteria of histological lung injury score

	No injury	25% injury	50% injury	75% injury	Diffuse injury
Edema	0	1	2	3	4
Inflammation	0	1	2	3	4
Bleeding	0	1	2	3	4

CO_2. Then, 2 mg/mL LPS was administered into HPMECs in six-well plates. The final concentrations of EX527 and SRT1720 are 15 and 30 μM, respectively [29]. SIRT1-small interference RNA (siRNA) were reverse transfected at a concentration of 40 nm with Transfection Reagent (Santa Cruz, USA) diluted in siRNA Transfection Medium (Santa Cruz, USA). After 8 h, cells were stimulated with LPS or same volume of PBS to allow for gene silencing. The sequences of SIRT1-siRNAs are as follows: sense (5′-GCGGGAAUCC AAAGGAUAATT-3′) and antisense (5′-UUAUCCUUUGGAUUCCCG CTT-3′).

Measurements of endothelial barrier permeability

For permeability studies, HPMECs were grown on fibronectin-coated polyester Transwell-clear filters (3 μm pore size, 12 mm diameter, Corning Costar Corporation 3462, UK). EX527/SRT1720 was added into the upper chamber 12 h before LPS administration. 24 h later, 1 mg/mL fluorescein isothiocyanate (FITC)-dextran was administered in the upper chamber. Samples were obtained at 0, 1, 2, 3, and 4 h after stimulation of dextran from the lower compartment of the Transwell-chambers. Fluorescence intensity was measured with a fluorescence spectrophotometer (excitation, 495 nm; emission, 528 nm; Thermo Scientific Ltd, California, USA) [30]. The permeability index was defined as the value of the lower chamber divided by the value of the upper chamber.

Transendothelial electrical resistance (TEER) was measured to assess the integrative function of the monolayer barrier using an Evom2 epithelial voltohmmeter (World Precision Instruments, Sarasota, USA) [31] with polyester Transwell-clear filters (0.4 μm pore size, 12 mm diameter; Corning Costar Corporation 3460, UK). TEER was calculated by the following formula: $\mathrm{TEER} = (\mathrm{TEER_A} - \mathrm{TEER_{blank}}) \times S_{\mathrm{membrane}}$, where $\mathrm{TEER_A}$ represents the TEER value for every experimental Transwell filter, $\mathrm{TEER_{blank}}$ represents the well without cells, and S_{membrane} represents the area of the filter membrane ($S = \pi \times r^2$; here $r = 6$ mm).

mRNA expression

For RNA extraction and quantitative reverse transcription polymerase chain reaction (RT-PCR) analysis, total RNA was extracted from tissues of mice using Trizol (Invitrogen, California, USA). High-fidelity cDNA was generated from each RNA sample using the Superscript III cDNA amplification system (Invitrogen, California, USA). Quantitative RT-PCR reaction samples were prepared as a mixture using the Quantitect SYBR Green PCR kit (Qiagen, Dusseldorf, Germany) following the manufacturer's instructions. Reactions were performed using an Applied Biosystems Prism 9700 PCR machine. The PCR conditions were as follows: 95 °C for 30 s followed by 45 cycles of 95 °C for 15 s, 55 °C for 30 s, and 72 °C for 30 s.

Western blot

Total protein was extracted from mice or cells. Protein concentration was determined using the BCA Protein Assay kit (Beyotime Biotechnology, China). Then, 30 μg protein in each group was separated by electrophoresis on 10% polyacrylamide sodium dodecyl sulfate gels and transferred to polyvinylidene difluoride membranes. The membranes were blocked for 1 h at room temperature with 5% bovine serum albumin and then incubated overnight at 4 °C with the following antibodies: SIRT1 (1:500, Abcam, Cambridge, USA), occludin (1:500, Abcam, Cambridge, USA), ZO-1 (1:200, Proteintech, China), ZO-2 (1:200, Proteintech, China), and GAPDH (1:1000, Abcam, UK). On the next day, membranes were washed and incubated with second antibody (1:4000, Beyotime Biotechnology, China) for 1 h at room temperature. After washing, the membranes were detected using an imaging system (Bioworld, California, USA). The obtained images were analyzed using Image Lab software.

Immunohistochemistry staining

Formalin-fixed paraffin-embedded tissue sections were dewaxed, hydrated, heated for 10 min in a conventional pressure cooler, treated with 3% H_2O_2 for 20 min, and then incubated with normal goat serum for 30 min. Histological slices were stained with SIRT1 (1:200, Abcam, USA), occludin (1:200, Abcam, USA), ZO-1 (1:200, Proteintech, Chicago, USA) and ZO-2 (1:200, Proteintech, Chicago, USA). The negative control was stained with same volume of PBS. After washing, the sections were incubated with biotin-labeled secondary antibody for 60 min at 37 °C. The color reaction was developed with a 3,3′-diaminobenzidine tetra-hydrochloride incubation. Slides were counterstained with hematoxylin, and then a cover slip was placed on slides. Immunohistochemistry (IHC) results were independently assessed by two pathologists who were blinded to STAT6 genotypes and clinico-pathological data. We employed the multiplicative quick score method (QS) to assess the expression of SIRT1 and occludin proteins. This system accounts for both the intensity and the extent of cell staining. In brief, the proportion of positive cells was estimated and given a percentage score on a scale from 1 to 6 (1 = 1–4%; 2 = 5–19%; 3 = 20–39%; 4 = 40–59%; 5 = 60–79%; and 6 = 80–100%). The average intensity of the positively staining cells was given an intensity score from 0 to 3 (0 = no staining; 1 = weak, 2 = intermediate, and 3 = strong staining) [32]. The QS was then calculated by multiplying the percentage score by the intensity score to yield a minimum value of 0 and a maximum value of 18.

Immunofluorescence

Fresh lung tissue was sliced into frozen sections. Sections were incubated with 0.2% Triton X-100 in PBS for 10 min followed by 5% bovine serum albumin for 1 h at room temperature. The slides were then incubated with antibodies at 4 °C overnight (claudin-5, Abcam, Cambridge, diluted 1:100). After washing, the slides were incubated with FITC-labeled secondary antibody for 60 min at 37 °C. Slides were counterstained with DAPI, and then a cover slip was placed on slides.

Statistical analysis

Data were expressed as the mean ± SEM and were analyzed by non-paired *T* tests. All the statistical analyses were performed using GraphPad Prism 5 (GraphPad Software Inc., La Jolla, CA, USA). $P < 0.05$ was considered to be statistically significant.

RESULTS

LPS reduced SIRT1 expression in mice

To assess the role of SIRT1 in LPS-induced ALI, SIRT1 expression in mice was measured. In vivo, LPS reduced SIRT1 expression by 36 % in the lung of mice compared with mice injected with the same volume of normal saline ($P < 0.01$). Comparing with the group of control (mice injected with normal saline), EX527, a selective inhibitor of SIRT1, significantly reduced SIRT1 gene expression by 50% and SRT1720, a selective activator of SIRT1, upregulated SIRT1 gene expression by 115%. Under LPS stimulation, EX527 significantly suppressed the expression of SIRT1 compared with the group of mice receiving only LPS ($P < 0.05$), whereas SRT1720 activated SIRT1 (Fig. 1a). IHC staining demonstrated that SIRT1 was mainly expressed in the cytoplasm and cyto-membrane of bronchial endothelial cells and rarely expressed in interstitial cells in the lung (Fig. 1b). QS results of IHC revealed that the addition of target depressor suppressed SIRT1 expression. In the LPS-induced mice, minimal visible positive SIRT1 expression in the lung was observed when inhibitor was injected. In contrast, the activator promoted pulmonary SIRT1 expression (Fig. 1c). SIRT1 levels detected by Western blot revealed the same alteration trend as RT-PCR (Fig. 1d). Molecular expression of SIRT1 in the group of EX527 was twice less than the control, whereas SRT1720 increased the expression by 34% compared with control. Figure 1e

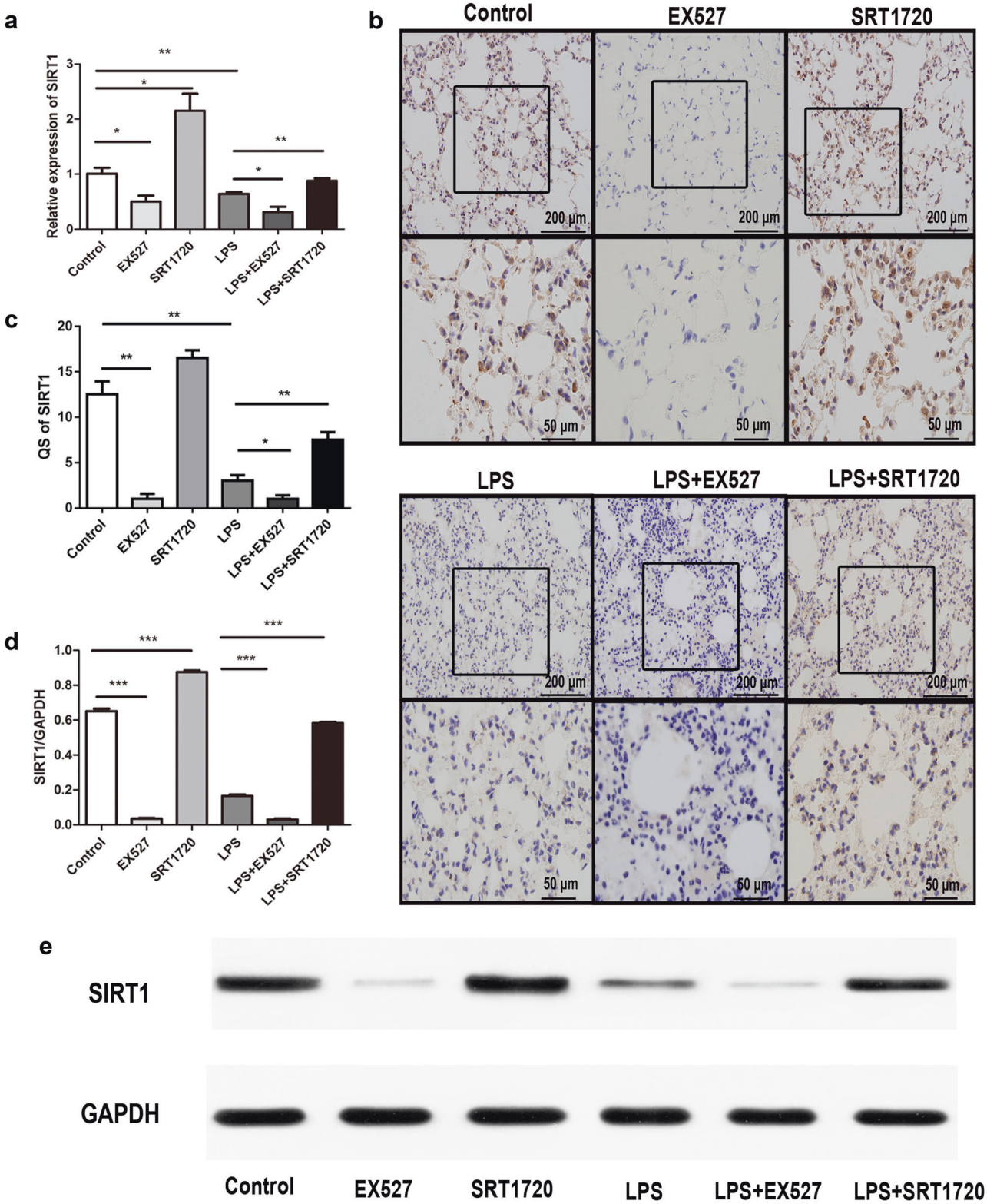

Fig. 1 LPS decreased SIRT1 expression in mice. **a** Relative expression of SIRT1 mRNA in different groups of mice (control, 10 mg/kg LPS intratracheally induced mice, 6.25 mg/kg of EX527, 6.25 mg/kg of SRT1720 alone or with LPS treatment). **b** Representative images of SIRT1 expression in IHC staining in six different groups. **c** Statistical IHC score of SIRT1 calculated using the multiplicative quick score method (QS). **d** Histograms represented the quantitative densitometric ratio of SIRT1 signaling molecules. **e** Representative Western blot images revealed SIRT1 expression. Data are expressed as the mean ± SEM. $^{*}P < 0.05$, $^{**}P < 0.01$, $^{***}P < 0.001$; $n = 6$ for each group. Similar results were observed for three independent experiments. LSD-t test was used in two comparisons between multiple data sets

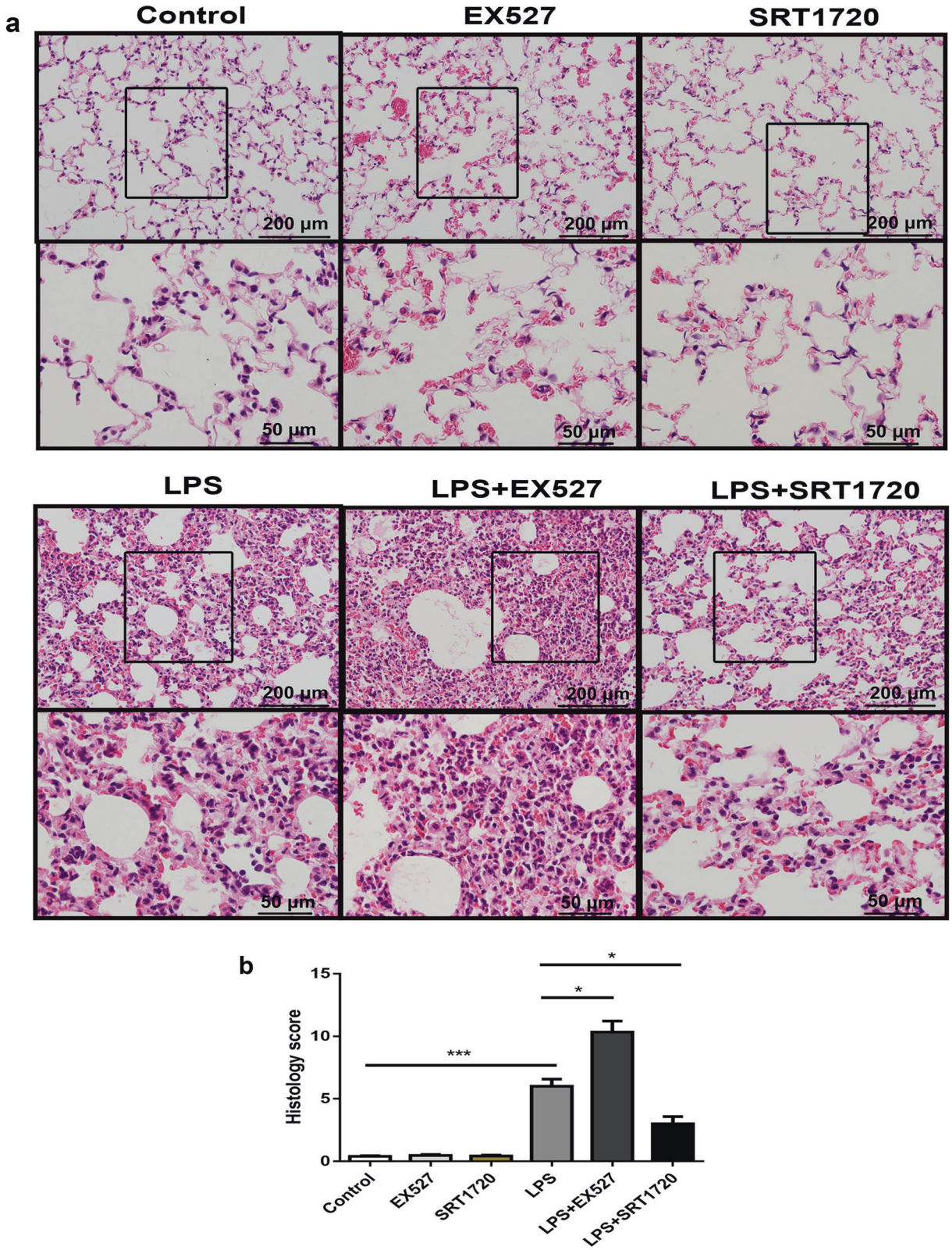

Fig. 2 A regulator of SIRT1 could influence LPS-induced lung injury. **a** Representative images of hematoxylin and eosin (H&E)-stained lung sections from six different groups. **b** Pathologic score results of lung section in these six groups. $^{*}P < 0.05$, $^{***}P < 0.001$. Data are expressed as the mean ± SEM. $n = 6$/group. Similar results were observed in three independent experiments. LSD-t test was used in two comparisons between multiple data sets

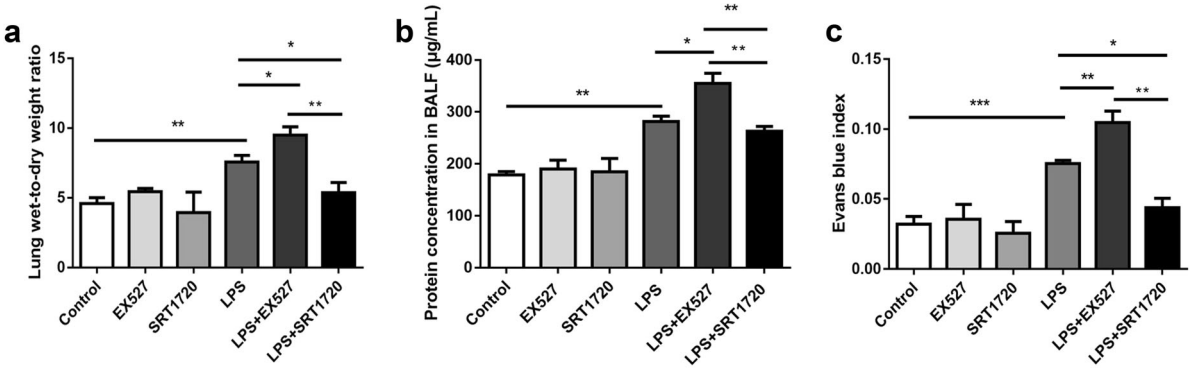

Fig. 3 SIRT1 regulated pulmonary permeability in LPS-induced ALI. **a** Lung wet/dry ratio of mice. **b** Bronchoalveolar lavage fluid (BALF) protein concentration measured using the BCA kit. **c** Evans blue index. *$P < 0.05$, **$P < 0.01$, ***$P < 0.001$. Data are expressed as the mean ± SEM. $n = 6$/group. Similar results were observed in three independent experiments. LSD-t test was used in two comparisons between multiple sets of data

presents the representative target band of SIRT1 compared with GAPDH. Taken together, EX527 and SRT1720 were an effective inhibitor and activator of SIRT1, respectively, and SIRT1 might play an important role in LPS-induced ALI.

SIRT1 regulated pulmonary permeability in LPS-induced ALI mice

LPS induced obvious lung injury with inflammatory cell infiltration in the interstitial and alveolar space, hemorrhage, edema, and the thickened alveolar wall compared with normal histomorphology in the control group. Compared with the LPS group, LPS plus the SIRT1 activator (SRT1720) alleviated lung injury, whereas LPS plus the SIRT1 inhibitor (EX527) aggravated lung injury. The SIRT1 activator or inhibitor alone did not exhibit visible histologic disparity in the lung (Fig. 2a). These changes were certified by statistical histology scores presented in Fig. 2b. In all, LPS could cause significant lung injury, and SIRT1 played a protective role in LPS-induced ALI.

To further explore the mechanism of the protective effect of SIRT1 on lung injury, the change of pulmonary permeability was assessed in vivo. The lung wet/dry ratio in the LPS group increased dramatically compared with the control group (Fig. 3a). An increased concentration of protein was noted in the BALF (Fig. 3b) and increased Evans blue leakage (Fig. 3c) was noted in the LPS group compared with the control ($P < 0.01$). In the presence of LPS, SRT1720 reduced the lung wet/dry ratio, decreased protein concentration in BALF and prevented Evans blue leakage in LPS-induced ALI mice. On the contrary, the lung wet/dry ratio, the protein concentration in BALF and Evans blue leakage significantly increased in LPS plus EX527 mice (Fig. 3a–c). Taken together, LPS-induced pulmonary hyper-permeability leading to lung injury, whereas SIRT1 alleviated lung injury through decreasing pulmonary permeability.

SIRT1 suppressed LPS-induced transmembrane permeability in vitro

To further verify the effect of SIRT1 on pulmonary cellular permeability, HPMECs were cultured in vitro. The destruction of the integrity of the endothelial barrier caused by LPS (control vs. LPS, 226.54 ± 29.41 ohm.cm^2 vs. 147.81 ± 24.14 ohm.cm^2) as evidenced by a significant reduction in the TEER was prevented upon pretreatment with SRT1720 (213.44 ± 48.98 ohm.cm^2). SRT1720 exhibited robust protective effects, whereas EX527 (107.8 ± 21.4 ohm.cm^2) decreased the TEER and increased the permeability of HPMECs (Fig. 4a). The speed of large molecules passing through cellular gaps is a good marker to detect cellular permeability. LPS significantly expedited fluorescein-labeled dextran passing across monolayers compared with control, and LPS plus EX527 further accelerated this process at each time point detected (1, 2, 3, and 4 h after the addition of dextran), whereas LPS plus SRT1720 significantly reduce the leakage of fluorescein-labeled dextran (Fig. 4b). These results suggest that SIRT1 protected endothelial barrier function from LPS-induced ALI. To exclude the nonspecific factors of inhibitors, siRNA was applied to certify the role of SIRT1 in endothelial cellular permeability. Specific siRNA was used to knock down SIRT1 expression. SIRT1 was effectively knocked down by 80% using siRNA (Fig. 4c). Under LPS stimulation, SIRT1 knockdown increased the TEER of HPMECs (Fig. 4d). Taken together, LPS induced hyper-permeability of HPMECs, whereas SIRT1 protected HPMECs from microvascular hyper-permeability.

SIRT1 decreased lung permeability through maintaining endothelial cellular tight junctions in ALI

To explore how SIRT1 affected the lung permeability, TJs were assessed in this study. Then, we attempted to determine the effect of SIRT1 regulators on the expression of occludin, ZO-1 and ZO-2. Figure 5a–c demonstrated that expression of occludin, ZO-1 and ZO-2 was reduced after LPS stimulation, and EX527 further downregulated the level of TJs. In contrast, SRT1720 restored the integrity of TJs (Fig. 5a–c). EX527 alone downregulated ZO-1 expression. Figure 5d, e further certifies this phenomenon by presenting the expression levels of TJs in HPMEC in vitro. Similar changes in TJs were also demonstrated utilizing Western blot. In the pathologic process of ALI, SIRT1 protected tight junction proteins from LPS-mediated injury.

In vivo, TJs were traced using IHC in LPS-induced ALI. The expression of occludin decreased in LPS-induced ALI mice, and EX527 further intensified this reduction. In contrast, SRT1720 elevated the expression of TJs induced by LPS (Fig. 6a, b). Minimal occludin was expressed in EX527-treated normal mice. Immunofluorescence (IF) staining revealed that claudin-5 was decreased after LPS stimulation, and activation of SIRT1 caused increased expression. SIRT1 inhibition caused reduced claudin-5 expression (Fig. 7a, b). Taken together, these data suggest that SIRT1 is a key regulatory factor of lung tight junction proteins, thus protecting endothelial permeability.

SIRT1 maintained LPS-induced tight junction permeability by targeting the RhoA/ROCK pathway

We found that RhoA and Rho-associated kinases (ROCK) signal levels were suppressed upon SIRT1 activation (Fig. 8a, b). The RhoA signal was upregulated in response to the SIRT1 inhibitor (Fig. 8c, d). The RhoA/ROCK signaling pathway plays important roles in this process. Y-27632, a RhoA/ROCK signal suppressor, was used to evaluate the role of this signal. Y-27632, with the concentration of 10 μM, significantly reversed LPS- or

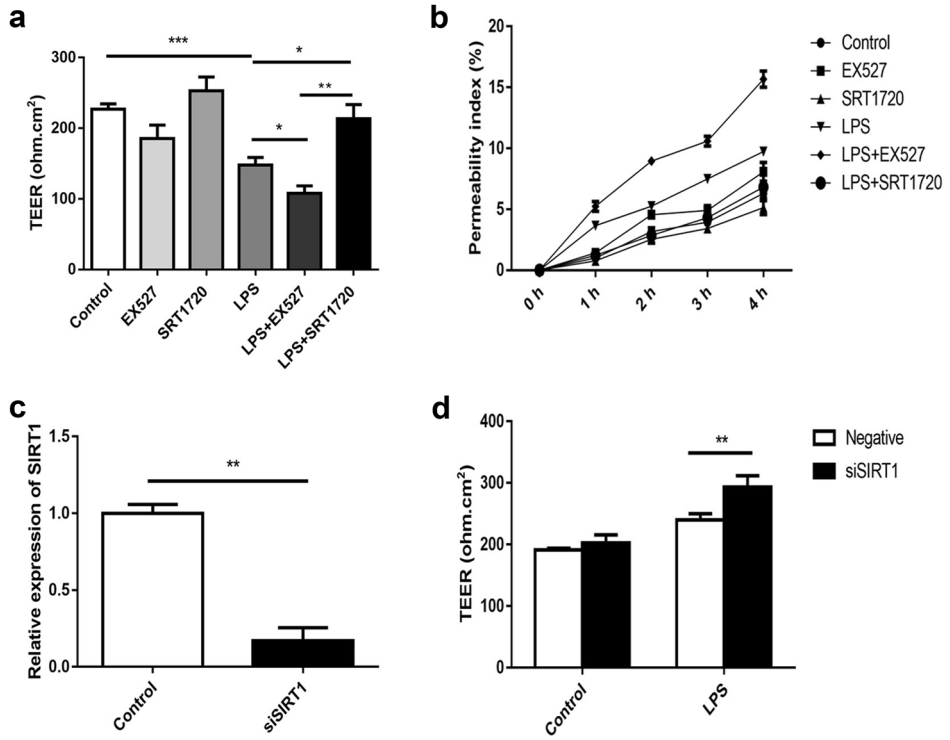

Fig. 4 SIRT1 regulated LPS-induced transmembrane permeability in vitro. **a** Value of TEER (ohm.cm^2) index of HPMECs among the group of control and different stimulation. **b** Permeability index of Transwell-membrane measured after the addition of FITC-dextran at 0, 1, 2, 3, and 4 h. **c** Knockdown of SIRT1 by siRNA. **d** Value of TEER between negative and siSIRT1 with/without LPS stimulation. *$P < 0.05$, **$P < 0.01$, ***$P < 0.001$. Data are expressed as the mean ± SEM. $n = 6$/group. Similar results were observed in three independent experiments. One-way ANOVA was used in multiple comparisons. LSD-t test was used in two comparisons between multiple data sets

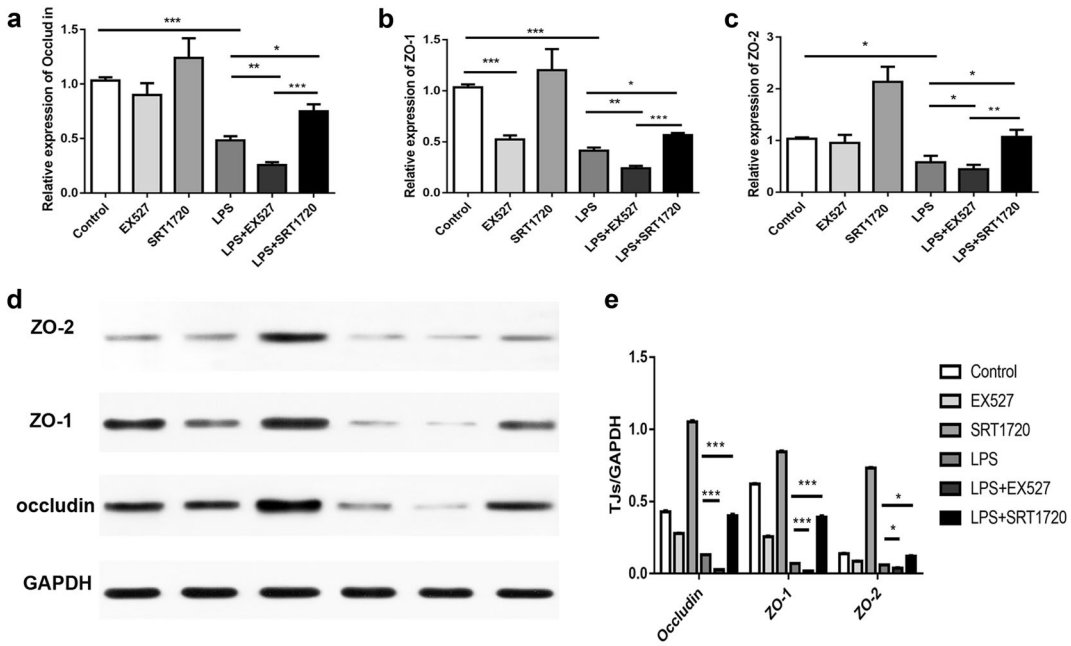

Fig. 5 Effect of a SIRT1 regulator on tight junction (TJs) protein expression. Relative gene expression of occludin (**a**), ZO-1 (**b**), and ZO-2 (**c**). **d** Representative image of Western blot of GAPDH, occludin, ZO-1, and ZO-2. **e** Histograms represented the quantitative densitometric ratio of target protein compared with GAPDH. *$P < 0.05$, **$P < 0.01$, ***$P < 0.001$. Data are expressed as the mean ± SEM. $n = 6$/group. LSD-t test was used in two comparisons between multiple data sets

EX527-induced hyper-permeability (Fig. 8e, f). These data suggest that the RhoA/ROCK signal could be a potential target of SIRT1. These data indicated that SIRT1 inhibited LPS-induced hyper-permeability by targeting the RhoA-ROCK pathway.

DISCUSSION

TJs in endothelial cells conferred key effects on the formation of normal barrier to balance lung permeability [33]. TJs form the intercellular barrier modulate intracellular signaling and

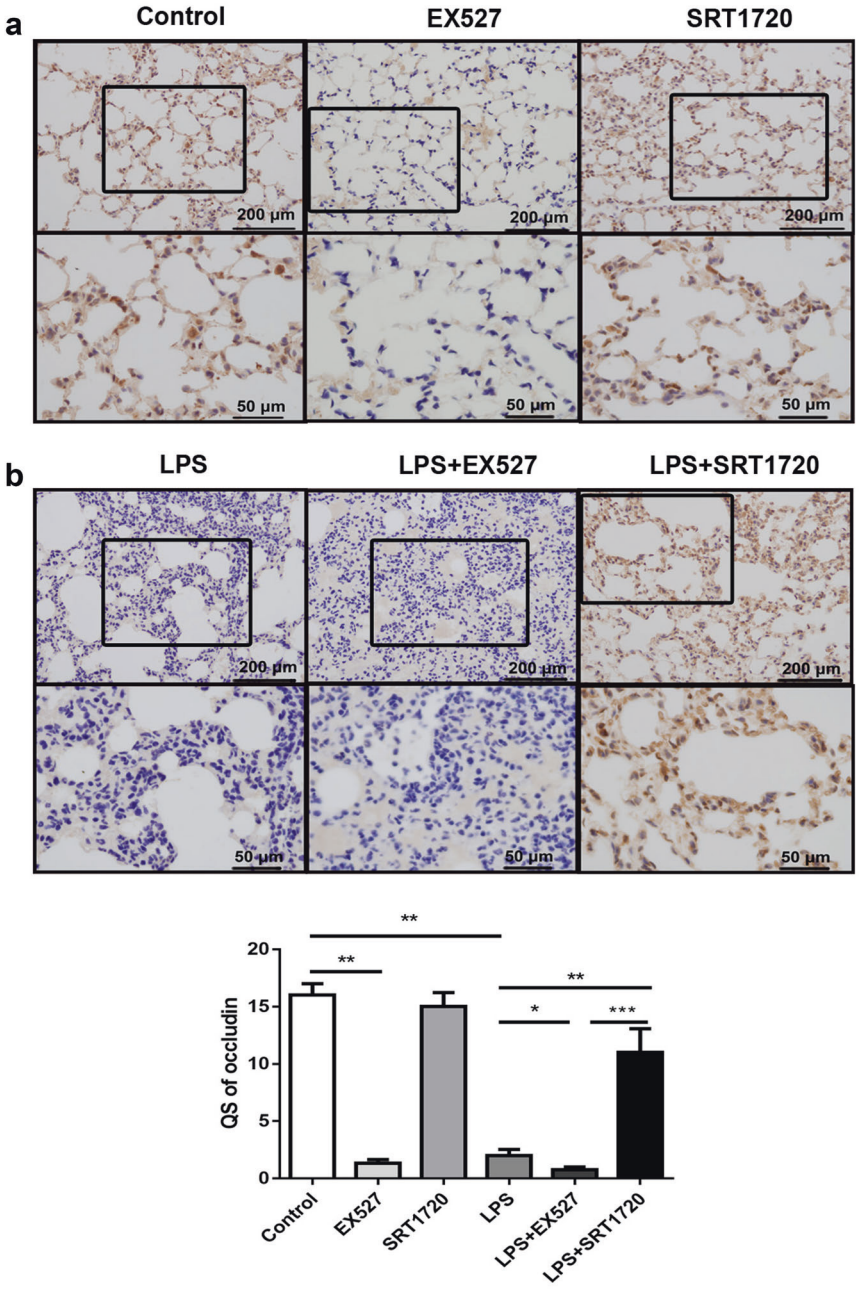

Fig. 6 Decreased occludin expression in the lung of LPS-induced mice. **a** Representative images of occludin expression based on IHC staining in different six groups. **b** Statistical IHC score of occludin calculated using the multiplicative quick score method (QS). $^{*}P < 0.05$, $^{**}P < 0.01$, $^{***}P < 0.001$. Data are expressed as the mean ± SEM. $n = 6$/group. Similar results were observed in three independent experiments. LSD-t test was used in two comparisons between multiple data sets

transportation to maintain normal lung barrier [34]. TJ damage would cause unbalanced lung permeability, thus contributing to lung injury [35]. SIRT1 acts on other TJ disruption-related pathologies, such as necrotizing enterocolitis, intestinal damage, viral transcription through the blood–brain barrier, metabolic kidney diseases and cell ageing [36–40]. Our findings indicated a previously unrecognized mechanism whereby SIRT1 reduced pulmonary TJ permeability and thus alleviated LPS-induced lung injury. Studies demonstrated that SIRT1 deficiency led to a dramatic reduction of lung claudin-1 and vascular endothelial-cadherin expression in mice and increased lung inflammasome activity during sepsis [41]. SIRT1 activation attenuated the reduced expression of TJs under hypoxia, indicating that SIRT1 maintains air–blood barrier function through regulating the expression of tight junctions under hypoxia [42]. One of the characteristics of ALI is malfunction of the normal barrier, thus leading to increased pulmonary permeability, accumulation of protein-rich edema in the alveoli and compromised lung vascular endothelium. The present study demonstrated that SIRT1 ameliorated LPS-induced hyper-permeability through regulating TJs. The results in this study further suggested that maintaining the expression level of tight junction proteins through targeting SIRT1 could be a potential therapy for ALI.

SIRT1 conferred effects both on lung inflammation and vascular permeability. Through upregulating SIRT1, resveratrol significantly reduced staphylococcal enterotoxin B-induced pulmonary vascular permeability, inflammation and downregulation of NF-kappaB in the inflammatory cells of the lungs [43]. Knockdown of SIRT1 by

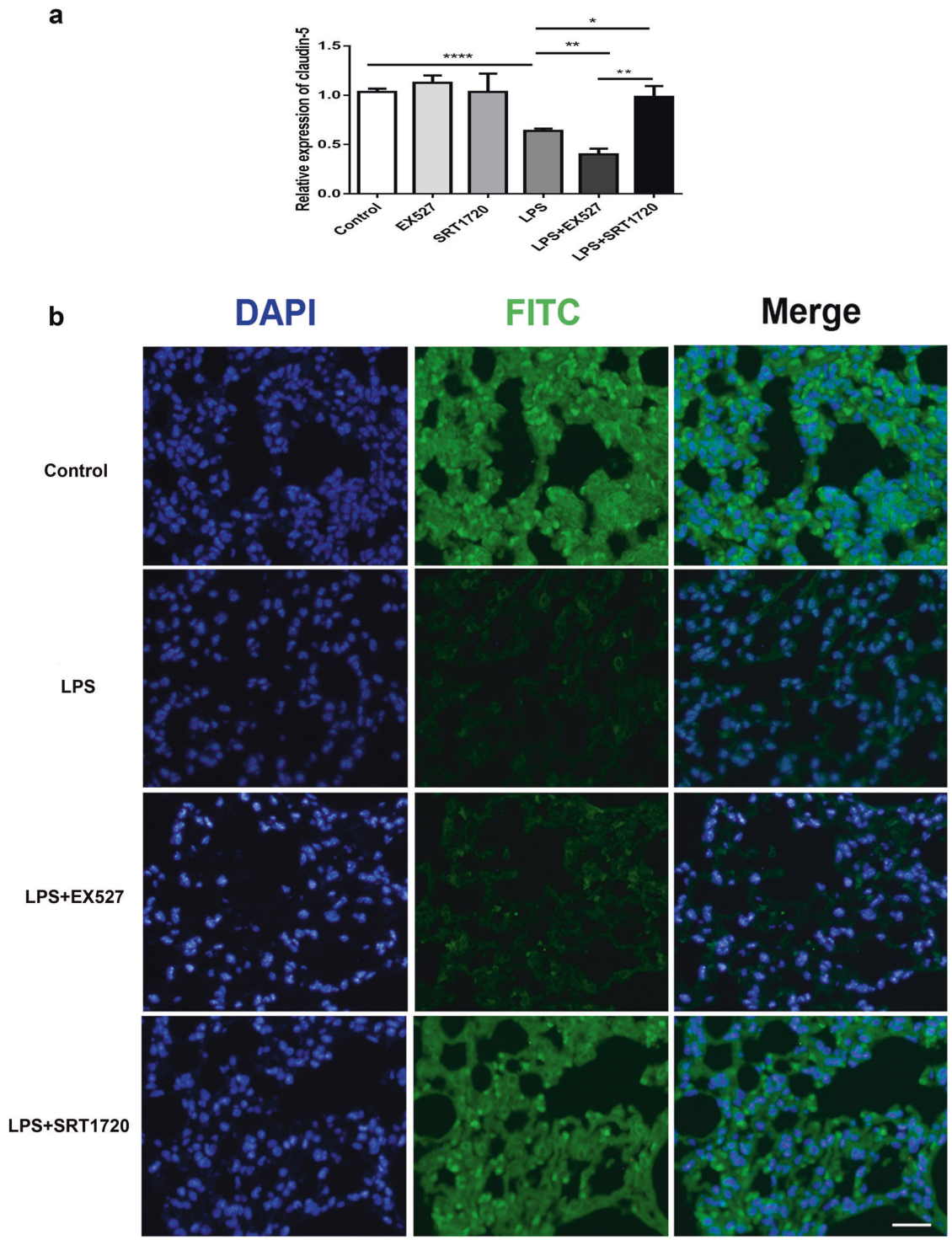

Fig. 7 SIRT1 regulates claudin-5 expression in the lung. **a**. Relative gene expression of claudin-5. *$P < 0.05$, **$P < 0.01$, ***$P < 0.001$. Data are expressed as the mean ± SEM. Scale bar = 50 μm. $n = 6$/group. LSD-t test was used in two comparisons between multiple sets of data. **b** Representative images of claudin-5 expression based on IF staining from four different groups

RNA interference resulted in increased cellular susceptibility to LPS stimulation and diminished the anti-inflammatory effect of resveratrol [44]. As shown in this study, SIRT1, especially under the pathologic condition induced by LPS, is an efficient target for the regulation of ALI and inflammation.

SIRT1 levels are maintained, at least in part, by RhoA activity in murine stem cells [45]. SIRT1 regulated dendritic development mediating the ROCK signaling pathway [46]. RhoA and ROCK also conferred effects on lung permeability and TJs. RhoA inhibition prevents both thrombin- and histamine-induced increases in endothelial permeability and decreases in trans-endothelial resistance. In addition, knockdown of RhoA not only inhibits stress fiber assembly and contractility but also prevents thrombin-induced disassembly of adherens and TJs in endothelial cells, indicating a role of RhoA in endothelial permeability [47]. RhoA stabilizes microvascular endothelial barrier functions in vitro and

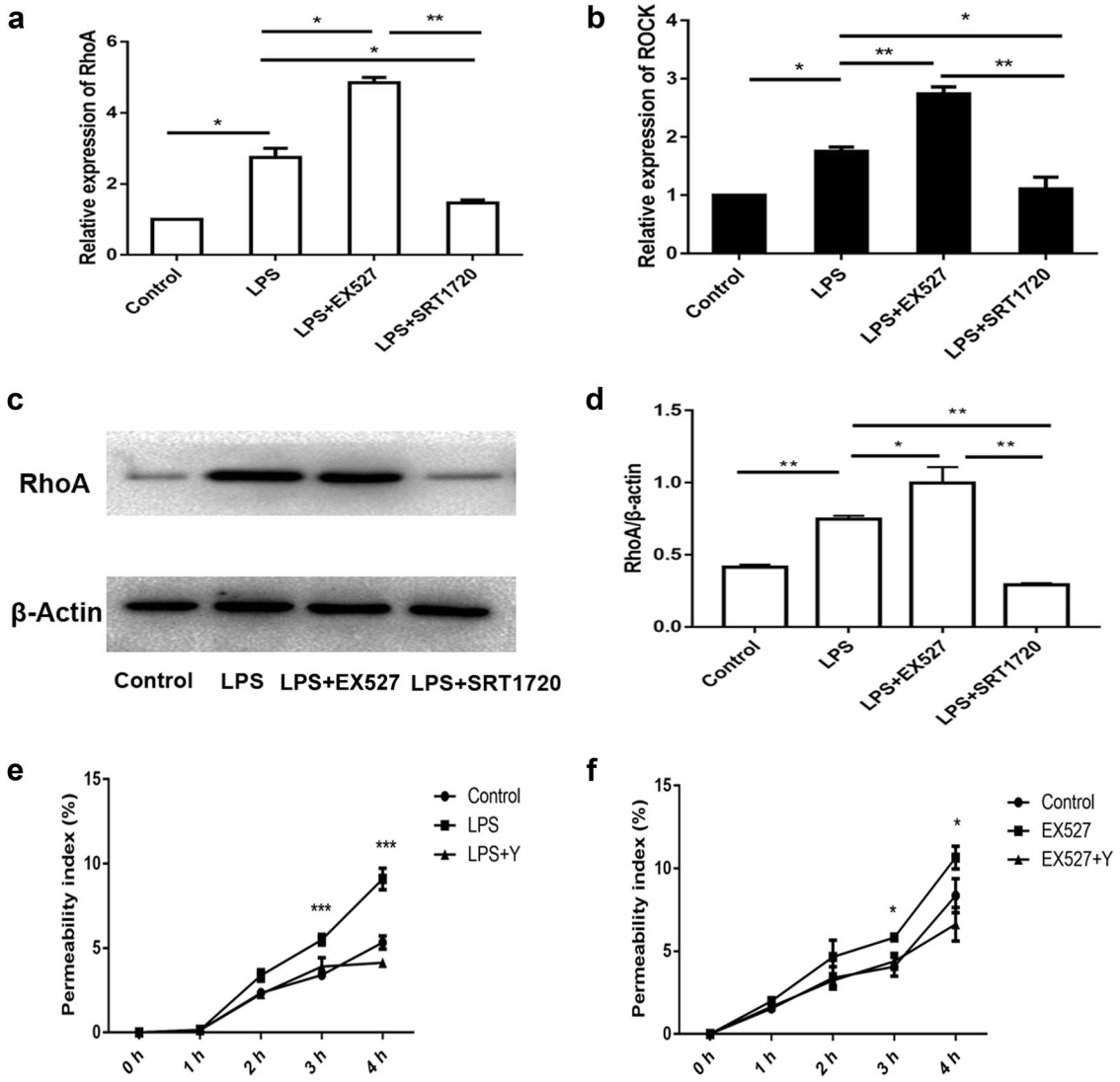

Fig. 8 SIRT1 acts on tight junction permeability through the RhoA/ROCK signal pathway. **a** Relative RhoA mRNA expression. **b** Relative ROCK mRNA expression. **c** Representative Western blot images of β-actin and RhoA. **d** Histograms represented the quantitative densitometric ratio of target protein compared with β-actin. **e**, **f** Permeability index of Transwell-membrane measured after the addition of FITC-dextran at 0, 1, 2, 3, and 4 h. $^{*}P < 0.05$, $^{**}P < 0.01$, $^{***}P < 0.001$. Data are expressed as the mean ± SEM. $n = 6$/group. Similar results were observed in three independent experiments. One-way ANOVA was used in multiple comparisons. LSD-t test was used in two comparisons between multiple data sets

in vivo likely by increasing the junction-associated actin cytoskeleton [48]. The RhoA/ROCK-mediated signaling pathway participated in LPS-induced hyper-permeability of HPMECs [49]. In our study, we observed that SIRT1 reduced LPS-induced RhoA activation and ROCK activity, which is consistent with the previous findings that RhoA/ROCK played an essential role in LPS-induced hyper-permeability [50]. Y-27632 reversed the hyper-permeability. The results described above suggest that SIRT1 preserved endothelial barrier homeostasis by targeting the RhoA/ROCK pathway.

Our study has several potential limitations. First, the blood–air barrier in the lung consists of the alveolar epithelial cells and underlying capillary endothelial cells. Our study exclusively focused on capillary endothelial cells, where a co-culture model may be applied to explore systemic mechanisms in future studies. Second, at the pharmaceutical level, both inhibitors and activators were adopted in vivo and in vitro in this study. At the genic level, apart from siRNA, over-expression studies might reveal further details regarding the systematic mechanism. Third, clinical transformation is the final goal of this research. Further exploration of ALI patients was suggested to certify the correlation between SIRT1 and TJ proteins for targeted medicine.

CONCLUSION

In summary, this study demonstrated that LPS-reduced SIRT1 expression levels negatively affected TJ proteins, and the RhoA/ROCK pathway played important roles in this process. Taken together, SIRT1 reduces lung vascular endothelial leakage through upregulating the expression of TJs, which may contribute to the development of new therapeutic approaches for pulmonary edema and other diseases caused by abnormal vascular permeability.

ACKNOWLEDGEMENTS

We thank Jie Liu at Shanghai Medical College, Fudan University for assisting in editing the language. This work was supported by grants from the National Natural Science

Foundation of China (No. 81472175, 81570081, 81770083 and 81300056), the National Key Research and Development Program of China (No. 2018YFC130103), the Zhejiang Provincial Natural Science Foundation of China (No. LY13H010002) and the Zhejiang Provincial Medical and Health Science and Technology Plan (No. 201353248).

AUTHOR CONTRIBUTIONS

C.F., H.L. and S.H. conceived and designed the experiments. C.F., Z.L. and S.H. performed the experiments. H.L. and L.W. analyzed the data. S.L. and W.J. contributed acquisition/materials. C.F., X.X. and J.Z. drafted the paper for revising it critically. All authors were approval of the submitted and final versions.

ADDITIONAL INFORMATION

Competing interests: The authors declare no competing interests.

Publisher's note: Springer Nature remains neutral with regard to jurisdictional claims in published maps and institutional affiliations.

REFERENCES

1. Matsuda N, Hattori Y, Takahashi Y, Nishihira J, Jesmin S, Kobayashi M, et al. Therapeutic effect of in vivo transfection of transcription factor decoy to NF-kappaB on septic lung in mice. Am J Physiol Lung Cell Mol Physiol. 2004;287: L1248–55.
2. Oshikawa K, Sugiyama Y. Gene expression of Toll-like receptors and associated molecules induced by inflammatory stimuli in the primary alveolar macrophage. Biochem Biophys Res Commun. 2003;305:649–55.
3. Yull FE, Han W, Jansen ED, Everhart MB, Sadikot RT, Christman JW, et al. Bioluminescent detection of endotoxin effects on HIV-1 LTR-driven transcription in vivo. J Histochem Cytochem. 2003;51:741–9.
4. Yi L, Huang X, Guo F, Zhou Z, Chang M, Tang J, et al. Lipopolysaccharide induces human pulmonary micro-vascular endothelial apoptosis via the YAP signaling pathway. Front Cell Infect Microbiol. 2016;6:133.
5. Rubenfeld GD, Caldwell E, Peabody E, Weaver J, Martin DP, Neff M, et al. Incidence and outcomes of acute lung injury. N Engl J Med. 2005;353:1685–93.
6. Tauseef M, Knezevic N, Chava KR, Smith M, Sukriti S, Gianaris N, et al. TLR4 activation of TRPC6-dependent calcium signaling mediates endotoxin-induced lung vascular permeability and inflammation. J Exp Med. 2012;209:1953–68.
7. Wojciak-Stothard B, Potempa S, Eichholtz T, Ridley AJ. Rho and Rac but not Cdc42 regulate endothelial cell permeability. J Cell Sci. 2001;114:1343–55.
8. Xing J, Wang Q, Coughlan K, Viollet B, Moriasi C, Zou MH. Inhibition of AMP-activated protein kinase accentuates lipopolysaccharide-induced lung endothelial barrier dysfunction and lung injury in vivo. Am J Pathol. 2013;182:1021–30.
9. Englert JA, Macias AA, Amador-Munoz D, Pinilla Vera M, Isabelle C, Guan J, et al. Isoflurane ameliorates acute lung injury by preserving epithelial tight junction integrity. Anesthesiology. 2015;123:377–88.
10. Gropper MA, Wiener-Kronish J. The epithelium in acute lung injury/acute respiratory distress syndrome. Curr Opin Crit Care. 2008;14:11–5.
11. Ahn C, Shin DH, Lee D, Kang SM, Seok JH, Kang HY, et al. Expression of claudins, occludin, junction adhesion molecule A and zona occludens 1 in canine organs. Mol Med Rep. 2016;14:3697–703.
12. Niessen CM. Tight junctions/adherens junctions: basic structure and function. J Invest Dermatol. 2007;127:2525–32.
13. Zemans RL, Colgan SP, Downey GP. Transepithelial migration of neutrophils: mechanisms and implications for acute lung injury. Am J Respir Cell Mol Biol. 2009;40:519–35.
14. Broermann A, Winderlich M, Block H, Frye M, Rossaint J, Zarbock A, et al. Dissociation of VE-PTP from VE-cadherin is required for leukocyte extravasation and for VEGF-induced vascular permeability in vivo. J Exp Med. 2011;208:2393–401.
15. Fang X, Neyrinck AP, Matthay MA, Lee JW. Allogeneic human mesenchymal stem cells restore epithelial protein permeability in cultured human alveolar type II cells by secretion of angiopoietin-1. J Biol Chem. 2010;285:26211–22.
16. Kojima K, Ohhashi R, Fujita Y, Hamada N, Akao Y, Nozawa Y, et al. A role for SIRT1 in cell growth and chemoresistance in prostate cancer PC3 and DU145 cells. Biochem Biophys Res Commun. 2008;373:423–8.
17. Ford J, Jiang M, Milner J. Cancer-specific functions of SIRT1 enable human epithelial cancer cell growth and survival. Cancer Res. 2005;65:10457–63.
18. Yeung F, Hoberg JE, Ramsey CS, Keller MD, Jones DR, Frye RA, et al. Modulation of NF-kappaB-dependent transcription and cell survival by the SIRT1 deacetylase. EMBO J. 2004;23:2369–80.
19. Singh UP, Singh NP, Singh B, Hofseth LJ, Price RL, Nagarkatti M, et al. Resveratrol (trans-3,5,4′-trihydroxystilbene) induces silent mating type information regulation-1 and down-regulates nuclear transcription factor-kappaB activation to abrogate dextran sulfate sodium-induced colitis. J Pharmacol Exp Ther. 2010;332:829–39.
20. Yang X, Jing T, Li Y, He Y, Zhang W, Wang B, et al. Hydroxytyrosol attenuates LPS-induced acute lung injury in mice by regulating autophagy and sirtuin expression. Curr Mol Med. 2017;17:149–59.
21. Smith LM, Wells JD, Vachharajani VT, Yoza BK, McCall CE, Hoth JJ. SIRT1 mediates a primed response to immune challenge after traumatic lung injury. J Trauma Acute Care Surg. 2015;78:1034–8.
22. Liu J, Yi L, Xiang Z, Zhong J, Zhang H, Sun T. Resveratrol attenuates spinal cord injury-induced inflammatory damage in rat lungs. Int J Clin Exp Pathol. 2015;8:1237–46.
23. Zhou XM, Zhang X, Zhang XS, Zhuang Z, Li W, Sun Q, et al. SIRT1 inhibition by sirtinol aggravates brain edema after experimental subarachnoid hemorrhage. J Neurosci Res. 2014;92:714–22.
24. Fu C, Jiang L, Xu X, Zhu F, Zhang S, Wu X, et al. STAT4 knockout protects LPS-induced lung injury by increasing of MDSC and promoting of macrophage differentiation. Respir Physiol Neurobiol. 2016;223:16–22.
25. Hong W, Xu XY, Qiu ZH, Gao JJ, Wei ZY, Zhen L, et al. Sirt1 is involved in decreased bone formation in aged apolipoprotein E-deficient mice. Acta Pharmacol Sin. 2015;36:1487–96.
26. Tager AM, LaCamera P, Shea BS, Campanella GS, Selman M, Zhao Z, et al. The lysophosphatidic acid receptor LPA1 links pulmonary fibrosis to lung injury by mediating fibroblast recruitment and vascular leak. Nat Med. 2008;14:45–54.
27. Su X, Bai C, Hong Q, Zhu D, He L, Wu J, et al. Effect of continuous hemofiltration on hemodynamics, lung inflammation and pulmonary edema in a canine model of acute lung injury. Intensive Care Med. 2003;29:2034–42.
28. Reutershan J, Morris MA, Burcin TL, Smith DF, Chang D, Saprito MS, et al. Critical role of endothelial CXCR2 in LPS-induced neutrophil migration into the lung. J Clin Invest. 2006;116:695–702.
29. Jia Y, Zheng Z, Wang Y, Zhou Q, Cai W, Jia W, et al. SIRT1 is a regulator in high glucose-induced inflammatory response in RAW264.7 cells. PLoS ONE. 2015;10: e0120849.
30. Ni Y, Teng T, Li R, Simonyi A, Sun GY, Lee JC. TNFalpha alters occludin and cerebral endothelial permeability: role of p38MAPK. PLoS ONE. 2017;12: e0170346.
31. Banks WA, Gray AM, Erickson MA, Salameh TS, Damodarasamy M, Sheibani N, et al. Lipopolysaccharide-induced blood-brain barrier disruption: roles of cyclooxygenase, oxidative stress, neuroinflammation, and elements of the neurovascular unit. J Neuroinflamm. 2015;12:223.
32. Melling N, Rashed M, Schroeder C, Hube-Magg C, Kluth M, Lang D, et al. High-level gamma-glutamyl-hydrolase (GGH) expression is linked to poor prognosis in ERG negative prostate cancer. Int J Mol Sci. 2017;18:E286.
33. Smith LS, Zimmerman JJ, Martin TR. Mechanisms of acute respiratory distress syndrome in children and adults: a review and suggestions for future research. Pediatr Crit Care Med. 2013;14:631–43.
34. Green KJ, Getsios S, Troyanovsky S, Godsel LM. Intercellular junction assembly, dynamics, and homeostasis. Cold Spring Harb Perspect Biol. 2010;2:a000125.
35. Yang J, Wang Y, Liu H, Bi J, Lu Y. C2-ceramide influences alveolar epithelial barrier function by downregulating Zo-1, occludin and claudin-4 expression. Toxicol Mech Methods. 2017;27:293–7.
36. Bein A, Zilbershtein A, Golosovsky M, Davidov D, Schwartz B. LPS induces hyper-permeability of intestinal epithelial cells. Pediatr Neonatol. 2017;232:381–90.
37. Wei W, Wang L, Zhou K, Xie H, Zhang M, Zhang C. Rhapontin ameliorates colonic epithelial dysfunction in experimental colitis through SIRT1 signaling. Int Immunopharmacol. 2017;42:185–94.
38. Castro V, Bertrand L, Luethen M, Dabrowski S, Lombardi J, Morgan L, et al. Occludin controls HIV transcription in brain pericytes via regulation of SIRT-1 activation. FASEB J. 2016;30:1234–46.
39. Wakino S, Hasegawa K, Itoh H. Sirtuin and metabolic kidney disease. Kidney Int. 2015;88:691–8.
40. Cheung TM, Ganatra MP, Peters EB, Truskey GA. Effect of cellular senescence on the albumin permeability of blood-derived endothelial cells. Am J Physiol Heart Circ Physiol. 2012;303:H1374–83.
41. Gao R, Ma Z, Hu Y, Chen J, Shetty S, Fu J. Sirt1 restrains lung inflammasome activation in a murine model of sepsis. Am J Physiol Lung Cell Mol Physiol. 2015;308:L847–53.
42. Li T, Zhang J, Feng J, Li Q, Wu L, Ye Q, et al. Resveratrol reduces acute lung injury in a LPS induced sepsis mouse model via activation of Sirt1. Mol Med Rep. 2013;7:1889–95.
43. Rieder SA, Nagarkatti P, Nagarkatti M. Multiple anti-inflammatory pathways triggered by resveratrol lead to amelioration of staphylococcal enterotoxin B-induced lung injury. Br J Pharmacol. 2012;167:1244–58.
44. Guo L, Li S, Zhao Y, Qian P, Ji F, Qian L, et al. Silencing angiopoietin-like protein 4 (ANGPTL4) protects against lipopolysaccharide-induced acute lung injury via regulating SIRT1/NF-kB pathway. J Cell Physiol. 2015;230:2390–402.

45. Yang J, Wu C, Stefanescu I, Jakobsson L, Chervoneva I, Horowitz A. RhoA inhibits neural differentiation in murine stem cells through multiple mechanisms. Sci Signal. 2016;9:ra76.
46. Codocedo JF, Allard C, Godoy JA, Varela-Nallar L, Inestrosa NC. SIRT1 regulates dendritic development in hippocampal neurons. PLoS ONE. 2012;7: e47073.
47. Wojciak-Stothard B, Tsang LY, Paleolog E, Hall SM, Haworth SG. Rac1 and RhoA as regulators of endothelial phenotype and barrier function in hypoxia-induced neonatal pulmonary hypertension. Am J Physiol Lung Cell Mol Physiol. 2006;290: L1173–82.
48. Waschke J, Burger S, Curry FR, Drenckhahn D, Adamson RH. Activation of Rac-1 and Cdc42 stabilizes the microvascular endothelial barrier. Histochem Cell Boil. 2006;125:397–406.
49. Huang Y, Tan Q, Chen R, Cao B, Li W. Sevoflurane prevents lipopolysaccharide-induced barrier dysfunction in human lung microvascular endothelial cells: rho-mediated alterations of VE-cadherin. Biochem Biophys Res Commun. 2015;468:119–24.
50. Li Y, Wu Y, Wang Z, Zhang XH, Wu WK. Fasudil attenuates lipopolysaccharide-induced acute lung injury in mice through the Rho/Rho kinase pathway. Med Sci Monit. 2010;16:Br112–8.